ISSN: 2688-8645

Numerical Analysis of Deformation and Mechanical Characteristics of Circular Suspended Footing Diaphragm Wall with Deep Tunnel

Danqing Zhang [1], Yushu Ding [2], Kefei Jiang [2], Bo Wang [2], Ning Li [2, 3, *]

[1] Shanxi Conservancy Technical Institute, Taiyuan Shanxi, 030027, China

[2] School of Environment and Architecture, University of Shanghai for Science and Technology, Shanghai 200093, China

[3] Key Laboratory of Geotechnical and Underground Engineering of the Ministry of Education, Tongji University, Shanghai 200092, China

* Corresponding author: Ning Li (Email: lining0017@usst.edu.cn)

Abstract

Research on circular suspended footing diaphragm walls in "soil-rock combination" strata remains underdeveloped. Understanding deformation and internal force variations during foundation pit excavation is crucial for mitigating safety risks during construction and operation. Based on a circular shaft pit in a water diversion project, this study employs 3D numerical simulations to analyze surface settlement, maximum pit bottom rebound, diaphragm wall deformation ,and internal forces under varying rock-socketed depths. Results indicate: (1) Excavation impacts surface settlement within 0.44H (H is the pit depth). The maximum rebound at the pit bottom in soft soil is significantly greater than that in rock. (2) Diaphragm wall horizontal deformation forms vary as "M," "bow," or "cantilever" with different embedded depths. (3) Large horizontal deformation, bending moments, and shear forces occur at the soil-rock interface and in weak rock strata. (4) Tunnel excavation minimally affects surface settlement and bottom rebound, while increasing maximum wall horizontal deformation by 0.35%–0.55%. However, wall removal in the tunnel area substantially impacts axial bending moments and shear forces. The research results can provide a reference for the design of retaining structure of similar soil rock combined foundation pit.

Keywords

Deep Buried Tunnel; Circular Foundation Pit; Hanging Foot Type Diaphragm Wall; Soil and Rock Combination Stratum; Deformation and Internal Force; Numerical Analysis.

1. Introduction

Currently, underground engineering construction in China is developing rapidly, and the number of foundation pits encountered in projects such as highways, railways, and bridges is increasing. The geological conditions of these foundation pits are becoming increasingly complex. The favorable load-bearing form of circular retaining structures has attracted considerable attention. Liu measured the wall deflection profile at the end of excavation, which showed a typical bulging type[1]. They described the relationship between normalized maximum wall deflection and safety factor. The observed maximum deflection of the retain-ing wall typically lies near the lower limit proposed by existing studies. Jia conducted a field monitoring study of the circular foundation pit of the Shanghai Tower, analyzing the variation patterns of lateral earth pressure, wall horizontal deformation, and other factors in circular diaphragm walls[2]. Cho combining experimental and two-dimensional numer-ical simulation studies, found that

ISSN: 2688-8645

the "arching effect" of circular diaphragm walls is more pronounced in soft soil layers compared to rock layers[3]. Borges conducted a numerical simulation study on the influence of parameters such as the elastic modulus of circular dia-phragm walls and the wall embedment depth on the internal forces and deformation of the wall[4]. He based on field measurements from an engineering site, proposed a method for predicting the deformation and internal force variation trends of circular diaphragm walls[5]. Keawsawasvong investigated the stability of circular diaphragm walls under excava-tion in heterogeneous clay layers by developing a numerical model[6]. Gao based on three-dimensional numerical simulations and field measurement data, studied the variation patterns of horizontal deformation in circular diaphragm walls[7]. Shi conducted nu-merical simulations to study a large circular deep foundation pit in Wuhan, analyzing the dis-tribution patterns of horizontal deformation and axial forces in its diaphragm wall under both distributed and simultaneous excavation conditions[8]. Wu based on three-dimensional numerical simulations, explored the impact of tunnel boring machine (TBM) crossing on circular diaphragm walls, analyzing the deformation and stress characteristics of the walls[9,10]. Guo established a three-dimensional numerical model of the interaction between the foundation pit, supporting structures, and buildings using the FLAC3D finite difference program[11]. They studied the effects of support structure materials, quantity, as well as the thickness and embedment depth of the retaining structure on its horizontal displacement. The results showed that as the number, stiffness, and thickness of the supports increased, the displacement of the retaining structure decreased. Additionally, the location of the maximum displacement of the retaining structure tended to develop downward as the embedment depth increased.

As mentioned above, many scholars have conducted extensive research on the founda-tion pit protection for vertical shafts in homogeneous soil or hard rock strata. In recent years, however, the protection of foundation pits in dual-layered strata, such as "soil over rock" in regions like Guangzhou and Qingdao, has also begun to attract widespread attention from scholars. Cantilever diaphragm walls do not require the wall to extend below the excavation depth of the foundation pit; it is sufficient to embed the wall into a stable rock layer. This ef-fectively utilizes the strength of the rock, making it highly suitable for the protection of foun-dation pits in soil-rock mixed strata. Chen based on site data from a foundation pit group, including lateral deflection of the retaining piles, ground settlement, and vertical column movement, concluded that the excavation of adjacent pits reduces the lateral deformation of the retaining structure[12]. Su studied the deformation and mechanical properties of square deep foundation pit support structures under soil-rock combined geological conditions[13]. Xu using field measurements and two-dimensional numerical simulations, studied the mechanical and deformation characteristics of foundation pit support structures in soil-rock combined strata in Jinan[14]. Zhang studied the distribution of lateral earth pressure on rock-embedded circular underground continuous walls [15]. Diao used the interface model in ABAQUS to simulate the interaction between the underground wall and the soil, investigating the effect of different friction angle δ parameters on the deflection of the continuous wall and surface settlement[16]. Tan studied a special type of foundation pit (a large circular pit with a small and deep rectangular pit excavated inside) and found that embedding the base of the circular diaphragm wall into the rock layer can reduce the defor-mation of the wall[17]. Although domestic and international scholars have achieved many mean-ingful results in the study of foundation pit protection structures in soil-rock combined strata, the diaphragm walls in these studies still use the same embedment depth into the rock. If the embedment depth of the diaphragm wall can be adjusted according to changes in the pit ge-ology, fully utilizing the stability of the rock layers, it could significantly reduce construction costs and project timelines [18].

In light of this, this paper combines the vertical shaft circular foundation pit engineering of an upcoming water diversion project, using finite element software to construct a three-

ISSN: 2688-8645

dimensional numerical model. The excavation process of the circular foundation pit and the deep-buried water diversion tunnel is simulated, and the deformation and stress characteristics of cantilever circular diaphragm walls with different embedment depths into the rock are analyzed. The research results can provide reference for the design and optimization of the embedment depth of diaphragm walls in similar deep-buried tunnel circular vertical shaft projects.

2. Engineering Overview

2.1. Engineering Background

The water plant distribution shaft for a water diversion project in Shenzhen is located south of Xinfeng Technology Park in Matian Street, Guangming District, Shenzhen, and also serves as a one-way launch shaft for the TBM. Its dimensions must meet the construction requirements of the TBM equipment and accommodate the arrangement of sectional maintenance butterfly valves, as well as the layout of butterfly and ventilation equipment. Therefore, a circular vertical shaft with an outer diameter of 34 meters is proposed. Due to the shallow burial depth of the bedrock at the project site, which features a typical soil-rock dual-layer stratum, a circular cantilever diaphragm wall is used as the retaining structure. The shaft structure also serves as an internal lining and is constructed using the top-down method. This circular shaft will connect with the deeply buried water diversion tunnel to meet the requirements of the water diversion project.

The shaft surface leveling elevation is 22.5m, while the bottom elevation of the foundation pit is -45m. The elevation of the deep water transmission tunnel stands at -35m, and its diameter measures 8m. The enclosure structure is a circular hanging diaphragm wall with an outer diameter of 21.2m and a wall thickness of 1.2m. The lining (at or above elevation -19.5m) has a thickness of 1.2m. Between elevations -19.5m and -22.5m, a full lining with a 1:1 slope is used, while the lining between elevations -22.5m and -45m has a thickness of 1.5m. The bottom of the vertical shaft consists of a 5m thick concrete slab. The different adjacent segments of the circular diaphragm wall are connected using the milling method, with 15 panels for both Phase 1 and Phase 2 segments. For the water diversion tunnel passage, the vertical shaft body is constructed with reserved openings, while the diaphragm wall in the tunnel area is constructed using blasting methods.

2.2. Hydrogeological Profile

According to the foundation pit geological survey data, the vertical shaft foundation pit is located in a "soil over rock" dual-layered strata. The soft soil layer primarily extends from a depth of approximately 30m to 40m, while the rock layers lie above 40m. The rock and soil layers involved in this circular vertical shaft foundation pit include: mixed fill, gravelly clay, completely weathered rock layers, strongly weathered rock layers, moderately weathered rock layers, fractured rock masses, strongly altered rock layers, weakly altered rock layers, and slightly weathered rock layers. The specific geological profile is shown in Figure 1, and the physical and mechanical parameters of the relevant geotechnical materials are presented in Table 1.

3. Finite Element Model

3.1. Computational Model

For major projects, to prevent accidents caused by design or construction errors, a feasibility analysis of the design and construction plans should be conducted through numerical simulations before the project begins. This paper combines an upcoming vertical shaft foundation pit project, and using ABAQUS commercial finite element software, establishes a

ISSN: 2688-8645

three-dimensional model that includes the strata, diaphragm walls, and vertical shaft (as shown in Figure 2). The model uses hexahedral solid elements (C3D8) for the geotechnical materials, diaphragm walls, and vertical shaft. The Mohr-Coulomb elastoplastic constitutive model is used for the geotechnical materials, while a linear elastic constitutive model is used for the diaphragm walls and vertical shaft due to their higher stiffness.

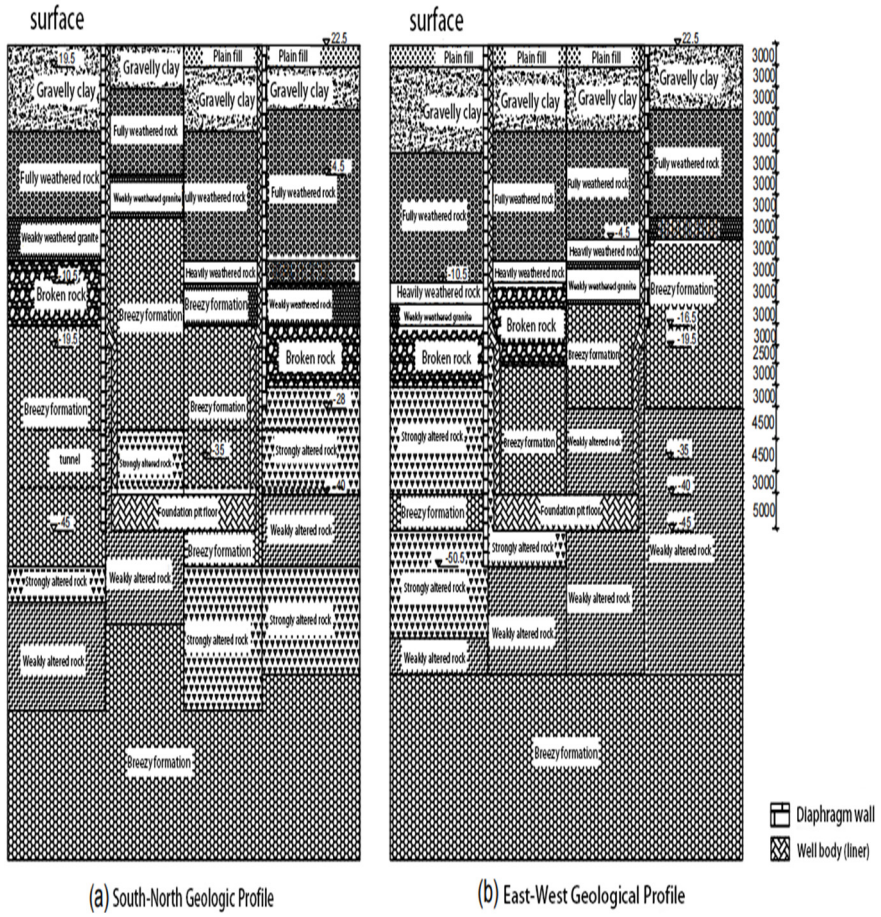

Figure 1. Geological profile sketch

Table 1. Physical and mechanical parameters of rock and soil mass

Rock Mass Name	Severty /g/cm³	Elasti Modulus /MPa	Cohesion /kPa	Internal Friction Angle /°	Poisson's Ratio
Plain fill	1.86	3.60	6	8	0.35
Gravelly clay	1.85	4.01	18	18	0.3
Completely Weathered rock	1.83	3.68	20	18	0.32
Heavily weathered rock	2.48	2×10^3	450	29	0.3
Weakly weathered rock	2.62	9×10^3	850	42	0.27
Breezy formation	2.61	17.5×10^3	1100	49	0.24
Strongly altered rock	2.51	1.5×10^3	360	29	0.29
Weakly altered rock	2.61	8×10^3	800	40	0.27
Fractured rock	2.51	1.5×10^3	350	28	0.29

To avoid the impact of model size on the final calculation results, according to the studies by Xu and Yao, the height of the foundation pit model should be 2-3 times the excavation depth, and

ISSN: 2688-8645

the width should be 2-4 times the excavation depth. Therefore, the computational domain of the numerical model for this vertical shaft foundation pit is 300m × 300m × 160m[19] [20].

At the same time, the coordinate system of the model is defined with the positive Y-axis pointing vertically upward, and the positive directions of the X-axis and Z-axis are determined based on the right-hand rule. All boundary conditions of the model are displacement boundary conditions. The upper surface of the model is a free surface, while the lower surface has fixed displacements in the X, Y, and Z directions. The left and right sides have fixed displacement in the Z direction, and the front and rear sides have fixed displacement in the X direction.

3.2. Simulation Methods and Construction Plan

The lining (vertical shaft body and diaphragm wall) parameters are: density of 2.4g/cm^3, elastic modulus of 31.5 GPa, and Poisson's ratio of 0.167. However, due to the use of the milling method in constructing the circular diaphragm wall, the joints between different wall segments reduce the overall stiffness of the wall. Therefore, a stiffness reduction factor is applied in the simulation to counteract the impact of the segment joints. The wall stiffness correction factor can be considered as the ratio between the composite wall stiffness and the stiffness of solid concrete. The stiffness correction factor for the diaphragm wall is a function of (2π)nr, where n is the number of joints in the entire circular cross-section, and r is the radius of the circular diaphragm wall. The calculated stiffness reduction factor for the diaphragm wall is 0.4. Other geotechnical material parameters are detailed in Table 1.

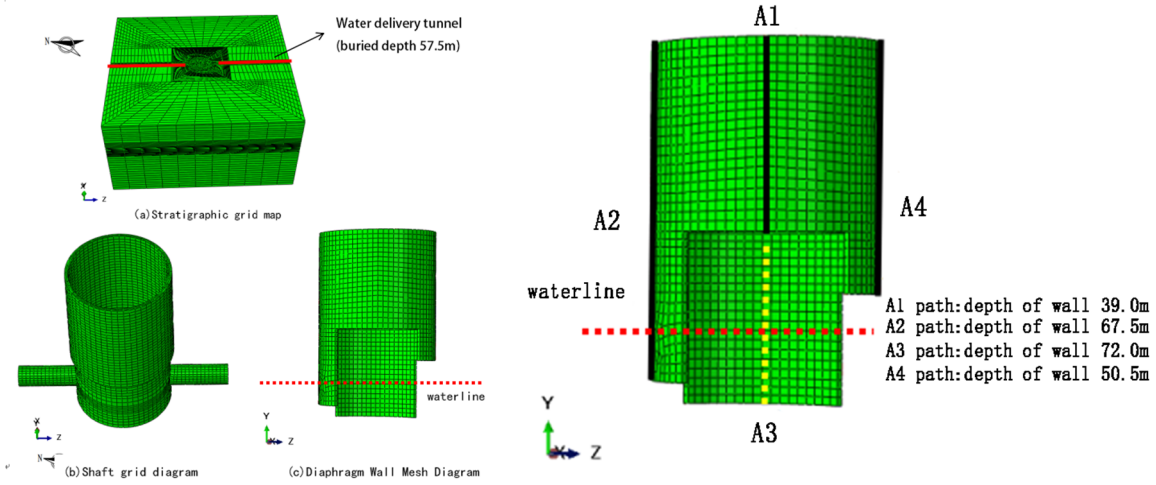

Figure 2. Numerical model of foundation excavation and Paths of the diaphragm wall

Previous studies have pointed out that when a displacement coordination model is used to simulate the interaction between the diaphragm wall and the soil, the computed results for wall deformation and internal forces are very close to the measured values [21]. Therefore, in this study, displacement constraints are used to simulate the interaction between different structures and between the structures and the geotechnical materials. The "death" element functionality is employed to simulate the excavation of geotechnical materials, the removal of the tunnel, the construction of the vertical shaft, and the lining of the water diversion tunnel.

Based on the excavation, shaft lining, and excavation and lining construction processes of the deep-buried tunnel, the model simulation will be divided into a total of 60 excavation steps: Excavation step 0 considers the effect of gravity initial stress field and balances the geostatic stress of the model; excavation steps 1 to 21 simulate the excavation of the foundation pit and the application of the shaft lining after excavation. After completing each excavation step, the corresponding shaft lining is applied as the inner lining. Steps 1 to 15 of the tunnel removal

ISSN: 2688-8645

simulate the excavation of the deep-buried tunnel and the application of the corresponding tunnel lining. The specific details of the excavation steps are shown in Table 2, where "Excavation" refers to the excavation of the corresponding soil layer in the foundation pit, "Inner lining" refers to the application of the corresponding shaft lining, "Remove tunnel" refers to the removal of the corresponding area of the water diversion tunnel, and "Lining" refers to the application of the tunnel lining. "Lining 0" represents the application of the shaft tunnel lining.

Table 2. Calculation Steps for Shaft Foundation Pit and Tunnel Excavation

Calculation step of excavation	content
Excavation 0	Ground Stress Balance
Excavation 1-16 Lining 1-16	Excavation Depth 3m, Apply Corresponding Wellbore After Excavation
Excavation 17, Lining 17	Excavation Depth 2.5m, Apply Wellbore
Excavation 18-19 Lining 18-19	Excavation Depth 4.5m, Apply Wellbore
Excavation 20, Lining 20	Excavation Depth 3m, Apply Wellbore
Excavation 21, Lining 21	Excavation Depth 5m, Pour Bottom Slab
Removal of Tunnel 1	Removal of Tunnel 1.5m
Removal of Tunnel 2	Removal of Tunnel 1.2m (Including Wall Tunnel) Destruction), Apply Lining 0
Removal of Tunnels 3-15	Removal of Tunnels 3-15 (Advance 1.5m), Apply Tunnel Lining 2-13
Lining 14-15	Apply Tunnel Lining 14-15

4. Three-dimensional-numerical-Analysis

4.1. Maximum Rebound Deformation Value at the Pit Bottom

Figure 3 shows the variation curve of the maximum rebound deformation value at the bottom of the foundation pit during excavation. As can be seen from Figure 3, before excavation condition 10 (excavation depth of 30m), there is a significant difference between the maximum rebound value at the bottom of the pit and the values at excavation condition 11 and beyond. This is due to the excavation of soft soil layers above a depth of 30m, where the strength of the soft soil is relatively weak, resulting in a large rebound during excavation. After this, the excavation primarily involves rock layers, which have relatively higher strength, resulting in smaller rebound values after excavation. This causes a significant difference between the two excavation sections. Furthermore, from Figure 3, it can be observed that during the entire excavation process, the maximum rebound value at the bottom of the pit exhibits a "N" shaped variation, first increasing, then decreasing, and then increasing again. This is because the soil layers above a depth of 15m (excavation steps 1-5) consist of loose fill and gravelly clay, which are very soft, while the depth from 15m to 30m mainly consists of completely weathered rock layers. Based on the geotechnical parameters provided in the geological report, it is evident that the strength of the completely weathered rock layer is marginally higher than that of the soft soil, leading to the maximum rebound deformation value initially increasing and subsequently decreasing during the excavation of this layer. When excavating more rigid rock layers, the rebound value gradually rises with the excavation progress. After the completion of the foundation pit base slab, the maximum rebound deformation value at the bottom of the pit decreased by 5.17%. Additionally, during the stages of tunnel removal and tunnel lining application, it can be clearly observed that the maximum rebound deformation value at the bottom of the pit remains largely stable and is not affected by the tunnel excavation.

ISSN: 2688-8645

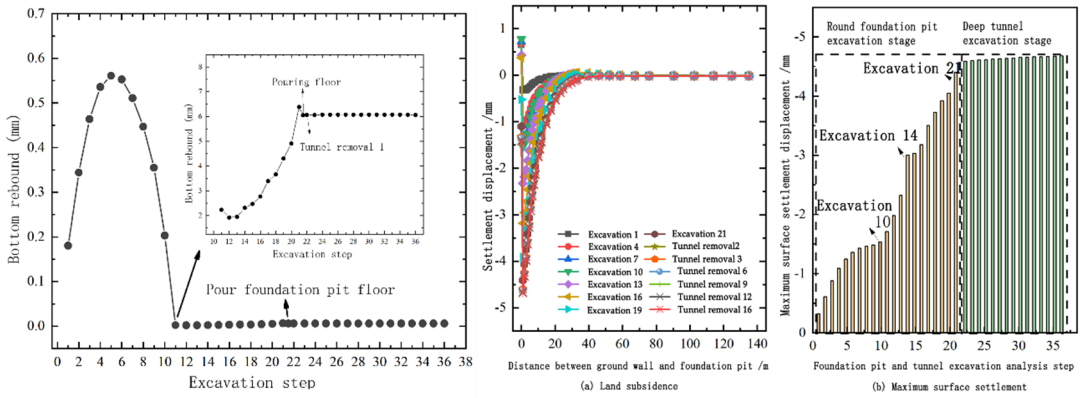

Figure 3. Maximum rebound deformation of foundation pit bottom and Surface settlement

4.2. Surface Settlement

Previous studies [23] have shown that excavation of a foundation pit can cause surface settlement around the pit, thus posing significant safety risks to surrounding buildings. Therefore, this section analyzes the variation pattern of surface settlement based on numerical simulation results. Figure 3(a) shows the variation of surface settlement displacement at different excavation analysis steps. From Figure 3(a), it can be seen that a typical "settlement trough" appears on the surface, showing a "bowl-shaped" distribution. The surface is significantly affected within a 30m (0.44H) range from the edge of the pit. As excavation progresses, the surface settlement value continues to increase, with the maximum settlement value reaching 4.68mm, occurring at approximately 3m (0.044H) from the pit. The soil at the pit edge undergoes upward deformation during the excavation of the soft soil layer. This is due to the bottom rebound pushing the diaphragm wall upwards, causing the soil connected to the wall to deform upward as well. Figure 3(b) shows the maximum surface settlement displacement at different analysis steps. From Figure 3(b), it can be seen that prior to excavation condition 10 (depth 30m), the rate of increase in surface settlement gradually decreases. The surface settlement increases at a rate of about 15% during excavation steps 11-14, and at a rate of about 5% during excavation steps 15-21. For the deep-buried tunnel excavation and lining application, after removing tunnel 1, the maximum surface settlement increased by 4.22%. Subsequently, the maximum surface settlement increased at a rate of about 0.22%. Overall, the impact of tunnel excavation on the settlement rate is minimal, which is due to the relatively deep-burial depth of the diversion tunnel, also indicating that the tunnel burial depth design is reasonably optimized.

4.3. Deformation and Stress Characteristics of Circular Diaphragm Walls

To clearly understand the deformation and stress characteristics of circular suspended diaphragm walls with different embedded rock depths based on complex geological designs, as well as the impact of deep tunnel excavation on the deformation and stress of the diaphragm wall. Based on the numerical simulation results, four wall paths, as shown in Figure 2, are selected to analyze their deformation and stress characteristics.

4.3.1. Horizontal Displacement

Figure 4(a) shows the variation of horizontal displacement along the A1 path wall (with a diaphragm wall depth of 39m) as the excavation of the pit and tunnel progresses. Figure 4(b) shows the distribution of the maximum horizontal displacement along the A1 path wall at each excavation analysis step. As seen in Figure 4(a), the horizontal displacement of the A1 path wall remains relatively unchanged along the wall depth throughout the excavation process of both the pit and deep tunnel, displaying a "bow-shaped" distribution. It is evident that after the wall is embedded in the rock layer, the horizontal displacement changes are minimal, indicating that

ISSN: 2688-8645

the rock layer can effectively suppress the horizontal deformation of the wall. During the excavation above a depth of 30m, the top of the wall primarily displaces outward from the pit, and then it begins to move inward toward the pit. As seen in Figure 4(b), the maximum horizontal displacement of the A1 path wall increases, then decreases, and increases again during the excavation process. This is due to the soft soil excavation before excavation condition 10, which releases a larger earth pressure, causing a continuous increase in the wall's horizontal displacement. When the excavation reaches the rock layer, the horizontal displacement suddenly decreases, and then increases again. This is because the stress released decreases when excavating from the soft soil layer to the rock layer, and the applied inner lining can also suppress the horizontal deformation of the wall. After the excavation of Tunnel 1, the maximum horizontal displacement of the wall increased by approximately 5.3%. Following the excavation of the deep buried tunnel, the maximum horizontal displacement of the wall increases at a rate of about 0.549%.

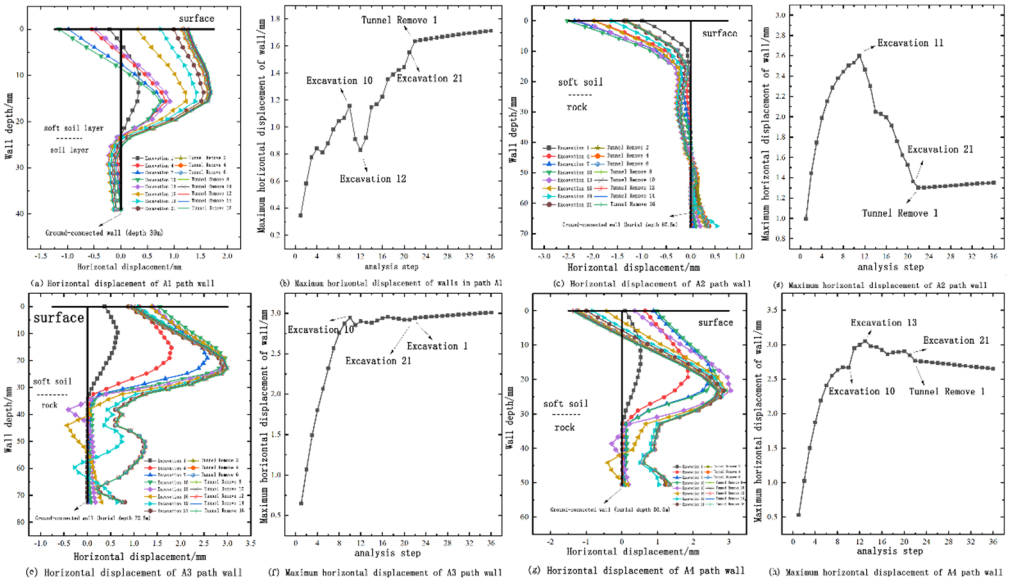

Figure 4. Horizontal displacement of A1-A4 path

Figure 4(c) shows the variation of horizontal displacement along the A2 path wall (with a diaphragm wall depth of 67.5m) as the excavation of the pit and tunnel removal progresses. Figure 4(d) shows the distribution of the maximum horizontal displacement along the A2 path wall at different excavation analysis steps. As shown in Figure 4(c), the horizontal displacement along the A2 path wall follows an overall "cantilever" shape, and the variation pattern does not change with the excavation of the pit or the removal of the tunnel. The "cantilever" shape is mainly due to the uneven geological strata, which causes the wall to shift outward from the pit. The maximum horizontal displacement occurs at the top of the diaphragm wall, with a maximum value of 2.6mm. As seen in Figure 4(d), the maximum horizontal displacement of the A2 wall shows an increasing-decreasing trend during the excavation of the pit. For the excavation of the rock layer, the wall's horizontal displacement consistently decreases, indicating that the application of the inner lining can effectively suppress the horizontal deformation of the wall. During the entire tunnel removal phase, the maximum horizontal displacement of the wall increases at a rate of approximately 0.368%.

Figure 4(e) shows the variation of horizontal displacement along the A3 path wall (with a diaphragm wall depth of 72.5m) as the excavation of the pit and tunnel progresses. Figure 4(f) shows the distribution of the maximum horizontal displacement along the A3 path wall at different excavation analysis steps. As shown in Figure 4(e), the horizontal displacement along

ISSN: 2688-8645

the A3 path wall follows an "M" shaped variation pattern with an initial increase, followed by a decrease, then an increase and decrease again. This is because the rock layers at depths 30-40m along the A3 path are mainly weakly weathered and minimally weathered rocks, which are relatively hard, leading to smaller changes in horizontal displacement. The rock layers at 40-60m depth are primarily fractured rocks and strongly weathered rocks, which are softer compared to the weakly weathered and minimally weathered layers. As excavation reaches this depth, the release of surrounding rock pressure from the outer pit causes the wall displacement to increase. The rock layer at the base of the wall is a minimally weathered layer, which is hard and stiff, leading to smaller horizontal displacement at the base. From Figure 4(f), it can be seen that the maximum horizontal displacement of the A3 path wall increases rapidly before excavation step 10, and then the overall trend shows a slow increase. During the tunnel excavation phase, the maximum horizontal displacement of the wall increases at a rate of approximately 0.463%.

Figure 4(g) shows the trend of horizontal displacement of the A4 path wall (with a depth of 50.5m) during the excavation and tunnel removal. Figure 4(h) shows the maximum horizontal displacement of the A4 path wall at different excavation analysis steps. From Figure 4(g), it can be seen that the wall displacement still follows an "arched" pattern with depth. After excavation step 16, the horizontal displacement at the wall base begins to increase, because excavation step 17 has reached the base of the A4 path wall, and the rock layers between depths of 39.5m-47.5m are fractured, which have relatively weaker strength, causing a slight increase in horizontal displacement at the wall base of the A4 path. From Figure 4(h), it can be seen that the maximum displacement of the wall gradually increases before excavation step 13, and then starts to decrease slowly. During the entire excavation process of the deep-buried tunnel, the maximum horizontal displacement of the wall decreases at a rate of 0.829%. This indicates that the deep-buried tunnel excavation did not affect the horizontal deformation of the wall along this path, and the lining also played a suppressive role.

According to relevant studies [11], since the diameter of the circular shaft pit simulated in this case is no greater than 40m and the excavation depth exceeds 35m for the retaining structure, the reference limit for horizontal deformation is 0.05%H. Combining Figures 4, it can be seen that the maximum horizontal deformation of the circular diaphragm wall is approximately 3.1mm (0.005%H), which is much smaller than the horizontal deformation limit, occurring at a depth of 25m (0.37H). This indicates that the design of the circular suspended diaphragm wall is reasonable and can ensure safety during the excavation and construction process of the pit.

4.3.2. Axial Bending Moment and Shear Force of Circular Diaphragm Walls

Figure 5 shows the distribution pattern of axial bending moments along the wall depth for A1-A4 path walls at different analysis steps. Figure 6 shows the maximum positive and negative axial bending moments of the walls (A1-A4 paths) at different analysis steps. Figure 7 shows the envelope of the axial bending moments of the wall. The positive bending moment direction points towards the inside of the pit, while the negative bending moment points towards the outside of the pit. From Figure 5, it can be seen that the variation pattern of axial bending moments for walls with different rock embedding depths remains basically unchanged, whether during the excavation of the pit or the tunnel. The maximum axial positive bending moment and maximum negative bending moment of the diaphragm wall both occur on the A3 path wall (wall depth 72.5m), with the maximum positive bending moment value of 305.5 KN·m at a depth of about 40m (0.597H) and the maximum negative bending moment value of -194.03 KN·m at a depth of about 52m (0.776H). From Figure 6, it can be seen that after the removal of the tunnel in the A2 path wall (wall depth 67.5m), the axial positive bending moment increased by 9.61%, and the axial negative bending moment decreased rapidly by 50.93%, indicating that the axial bending moment is primarily directed towards the inside of the pit at this stage.

ISSN: 2688-8645

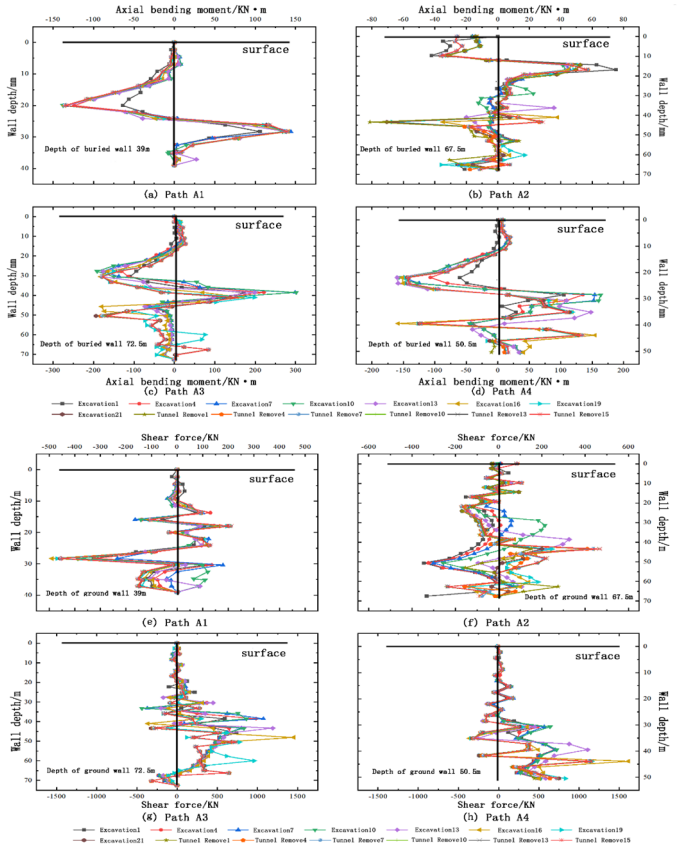

Figure 5. Axial bending moment and Shear force diagram of A1-A4 path of diaphragm wall under various excavation conditions

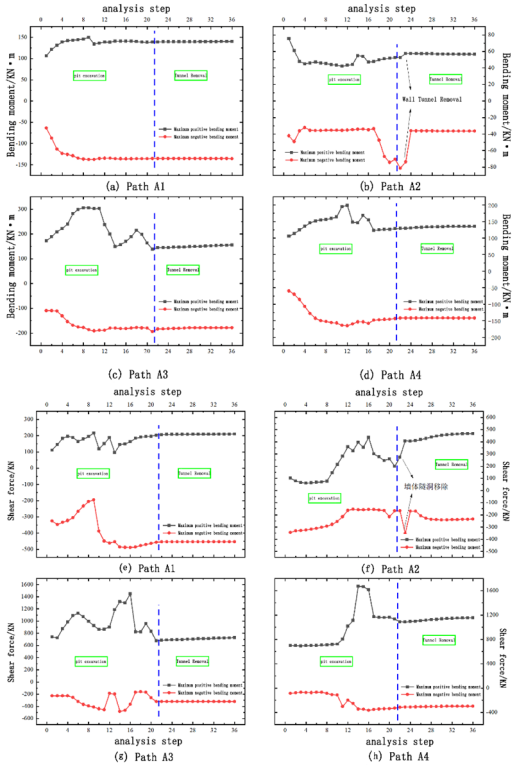

Figure 6. Maximum axial bending moment and Maximum shear force of A1-A4 of diaphragm wall under various excavation conditions

ISSN: 2688-8645

During the subsequent tunnel excavation, the maximum axial bending moments remain largely unchanged.

Based on Figure 7, the maximum positive bending moment for the upper section of the diaphragm wall (wall depth 0-25m) is approximately 75.25 KN·m, and the maximum negative bending moment is approximately 164.98 KN·m. The maximum positive bending moment for the middle section (wall depth 25-55m) is approximately 305.5 KN·m, and the maximum negative bending moment is approximately 194.03 KN·m. The maximum positive bending moment for the lower section (wall depth 55-72.5m) is approximately 75.98 KN·m, and the maximum negative bending moment is approximately 73.53 KN·m. The bending moments in the middle section of the wall are larger due to the presence of fractured rock layers. When the excavation reaches this depth, the released surrounding rock pressure is larger. Therefore, in the reinforcement design of the project, the steel reinforcement in the middle section should be strengthened, while the reinforcement in the upper and lower sections can be appropriately reduced to achieve cost savings in the project.

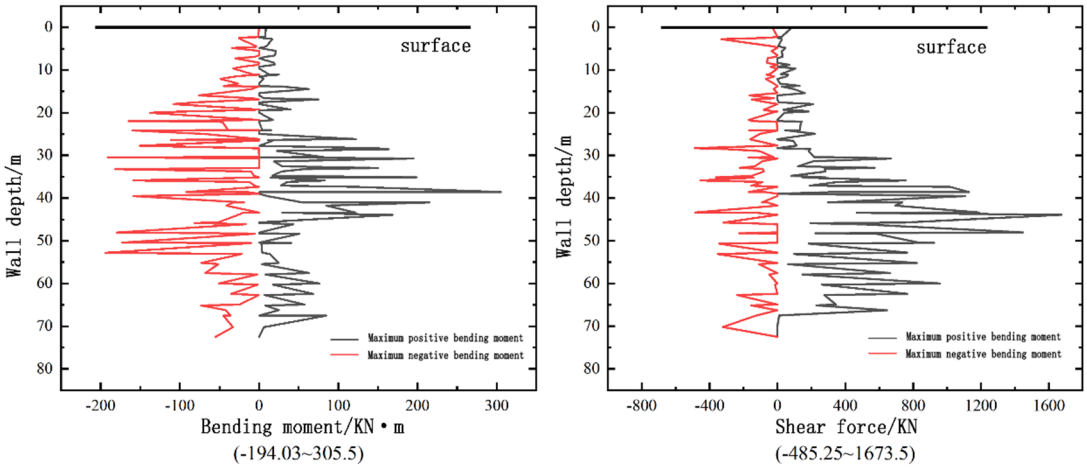

Figure 7. Bending moment and shear force envelope diagram

Figure 5 shows the distribution of shear force along the depth of the wall at different analysis steps for A1-A4 paths. Figure 6 shows the maximum positive and negative shear values at different analysis steps for the walls (A1-A4 paths). Figure 7 shows the shear force envelope for the walls. Positive shear force is directed toward the inside of the pit, and negative shear force is directed toward the outside of the pit. From Figure 5, it can be seen that the shear force distribution for walls with different embedded depths does not change significantly with the progression of excavation. The walls on the A3 (wall depth 72.5m) and A4 (wall depth 50.5m) paths mainly exhibit shear forces directed toward the inside of the pit. The maximum positive shear force for the diaphragm wall occurs on the A4 path wall, with a value of 1673.5 KN at a depth of approximately 44m (0.657H). The maximum negative shear force occurs on the A3 path wall, with a value of -485.25 KN at a depth of approximately 43m (0.642H). From Figure 6, it can be seen that during the tunnel removal phase, the overall rate of increase in shear force for the diaphragm wall is not significant. However, for the A2 path wall (wall depth 67.5m), after the tunnel removal, the positive shear force increased by 48.14%, and the negative shear force increased by 110.86%. Subsequently, the shear force during the tunnel excavation steps remained relatively unchanged. This is due to the damage to the integrity of the wall, causing a rapid increase in the shear force.

Referring to Figure 7, the maximum positive shear force in the upper section of the diaphragm wall (wall depth 0-25m) is 220.38 KN, and the maximum negative shear force in the upper

ISSN: 2688-8645

section is 331.75 KN. The maximum positive shear force in the middle section of the diaphragm wall (wall depth 25-55 m) is 1673.5 KN, and the maximum negative shear force is 485.25 KN. The maximum positive shear force in the lower section of the diaphragm wall (wall depth 55-72.5 m) is 767.25 KN, and the maximum negative shear force is 322.25 KN. Similar to the axial bending moment of the wall, the shear force in the middle section of the wall is also relatively large.

5. Conclusion

The maximum rebound deformation at the bottom of the pit in the soft soil layer excavation is much larger than that in the rock layer excavation. During the entire shaft pit excavation process, the maximum bottom rebound shows a fluctuating pattern. During the excavation process, the surface settlement outside the pit shows a “bowl-shaped” distribution, with the maximum settlement occurring at 0.044H, and the impact range on the surface outside the pit is approximately 0.44H.

For the horizontal deformation of the suspended circular diaphragm wall, due to the complex distribution of soil and rock geology and different embedded depths, the wall exhibits three different deformation patterns: "bow," "M," and "cantilever" shapes.

The axial bending moment and shear force of the diaphragm wall mainly show a trend of being small at both ends and large in the middle. The maximum values of bending moment and shear force mainly occur at the interface between soil and rock layers, as well as in the fractured rock layer and highly weathered rock layers, at wall depths of 40m-50m (0.59H-0.75H).

The excavation of the deeply buried tunnel has little impact on the bottom rebound and does not change the pattern of horizontal displacement of the wall. During the tunnel excavation, the maximum horizontal displacement of the wall increases at a rate of 0.35%-0.55%. When the diaphragm wall is broken in the tunnel area, due to the loss of wall integrity, the axial bending moment and shear force of the wall are significantly affected.

References

[1] Liu.N. W, Yu.F, Gong. X. N. Characteristics of Excavation-Induced Deformation Associated with Different Propped Retaining Walls in Soft Soil. In Pavement Materials and Associated Geotechnical Aspects of Civil Infrastructures: Proceedings of the 5th GeoChina International Conference 2018–Civil Infrastructures Confronting Severe Weathers and Climate Changes: From Failure to Sustainability, held on July 23 to 25, 2018 in HangZhou, China (pp. 21-34).Springer International Publishing.

[2] Jia. J, Zhai. J, Q. Li, , et al.Performance of large-diameter circular diaphragm walls in a deep excavation: Case study of Shanghai Tower. Journal of Aerospace Engineering, 32(5),04019078.

[3] Cho J, Lim. H, Jeong. S,et al.Analysis of lateral earth pressure on a vertical circular shaft considering the 3D arching effect. Tunnelling and Underground Space Technology, 48(2015), 11-19.

[4] Borges. J, L. Guerra, G. T. Cylindrical excavations in clayey soils retained by jet grout walls: Numerical analysis and parametric study considering the influence of consolidation. Computers and Geotechnics, 55 (2014), 42-56.

[5] He. W, Luo. C, Cui. J, et al. An axisymmetric BNEF method of circular excavations taking into account soil-structure interactions. Computers and Geotechnics, 90(2017), 155-163.

[6] Keawsawasvong. S, Ukritchon. B. Undrained basal stability of braced circular excavations in non-homogeneous clays with linear increase of strength with depth. Computers and Geotechnics (2019), 115, 103180.

[7] Gao. X, Tian. W. P, et al. Analysis of deformation characteristics of foundation-pit excavation and circular wall. Sustainability (2020), 12(8), 3164.

[8] Shi. H, Jia. Z, Wang. T, Cheng. Z, ,et al. Deformation characteristics and optimization design for large-scale deep and circular foundation pit partitioned excavation in a complex environment. Buildings(2022), 12(9), 1292.

[9] Wu. G, Jia. S, Chen. W, Yang. W, et al. Modelling analysis of the influence of shield crossing on deformation and force in a large diaphragm wall. Tunnelling and Underground Space Technology, 72 (2018), 154-161.

[10] Wu. G, Chen. W, Bian. H, et al. Structure optimisation of a diaphragm wall with special modelling methods in a large-scale circular ventilating shaft considering shield crossing. Tunnelling and Underground Space Technology, 65(2017), 35-41.

[11] Guo. J, Yang. Z, Dang. Y, et al. Deformation analysis of enclosure structure affected by foundation pit excavation. In Civil Engineering and Disaster Prevention (pp. 123-129). CRC Press.

[12] Chen. S, Cui. J, et al. Case study on the deformation coupling effect of a deep foundation pit group in a coastal soft soil area. Applied Sciences, 12(2022), 6205.

[13] Su. X. T, Zhang. Y. N, Zhang. X. X, et al. Deformation and Force Analysis of the Pile Foundation System of Deep Foundation Pits in Soil–Rock Combination. In IOP Conference Series: Earth and Environmental Science (Vol. 570 (2020), No. 6, p. 062041). IOP Publishing.

[14] Xu. Q, Bao. Z, Lu. T, et al. Numerical Simulation and Optimization Design of End-Suspended Pile Support for Soil-Rock Composite Foundation Pit. Advances in Civil Engineering, 2021(1), 5593639.

[15] Zhang. J, Li. M, Ke. L, et al. Distributions of lateral earth pressure behind rock-socketed circular diaphragm walls considering radial deflection. Computers and Geotechnics, 143 (2022), 104604.

[16] Diao. Y, Zheng. G, Numerical analysis of effect of friction between diaphragm wall and soil on braced excavation. Journal of Central South University of Technology, 15 (2008), 81-86.

[17] Tan. Y, Lu. Y, Xu. C, et al. Investigation on performance of a large circular pit-in-pit excavation in clay-gravel-cobble mixed strata. Tunnelling and Underground Space Technology, 79 (2018), 356-374.

[18] Qiao. Y, Xie. F, Bai .Z, et al. Deformation characteristics of ultra-deep circular shaft in soft soil: A case study[J]. Underground Space, 2024, 16: 239-260.

[19] Xu. Q, Bao. Z. Lu, et al. Numerical Simulation and Optimization Design of End-Suspended Pile Support for Soil-Rock Composite Foundation Pit. Advances in Civil Engineering, 2021(1), 5593639.

[20] Yao. C, Yan. Q, Sun. M, Dong. W, et al. Rigid diaphragm wall with a relief shelf to mitigate the deformations of soil and shallow foundations subjected to normal faulting. Soil Dynamics and Earthquake Engineering, 137 (2020), 106264.

[21] Barbero. E, J. Finite element analysis of composite materials using Abaqus®. CRC press.

[22] Sun.Y, Xiao.H, Wall displacement and ground-surface settlement caused by pit-in-pit foundation pit in soft clays. KSCE Journal of Civil Engineering, (2021).25(4).